Wave attenuation and focusing performance of parallel twin parabolic arc floating breakwater

Binzhen Zhou[a], Zhi Zheng[a], Peng Jin[b,*], Lei Wang[a], Jun Zang[c]

[a] *School of Civil Engineering and Transportation, South China University of Technology, Guangzhou 510641, China*

[b] *School of Marine Science and Engineering, South China University of Technology, Guangzhou 511442, China*

[c] *Department of Architecture & Civil Engineering, University of Bath, Bath, BA2 7AY, UK*

Abstract

The hybrid system consisting of floating breakwater and point absorber wave energy converters provides a promising solution for shoreline protection and wave power generation. In the hybrid system, the breakwater plays an important role in protecting the sheltered area on the lee side and focusing high waves for better energy harvesting on the weather side. To improve the wave attenuation and focusing performance, a twin-breakwater consisting of a pair of parallel parabolic pontoons is proposed. Based on the potential flow theory of linear waves, the influences of gap width and connection method applied between the two pontoons are studied in the frequency domain, with an emphasis on the so-called critical mode around which both wave attenuation and focusing could be improved. Results show that the rigidly connected twin-breakwater is superior to the unconnected twin-breakwater with the same configuration in both wave attenuation and focusing. A second critical mode with lower frequency is also found under particular gap width, providing a potential for the defense of long waves. An optimal attenuation could be obtained by applying a proper gap width.

Keywords: parabolic twin-breakwaters; wave energy; wave attenuation; wave focusing

1. Introduction

Wave power [1] is one of the most promising marine renewable energy resources [2][3] due to its vast capacity, high energy density, and predictability [4][5]. The exploitation of wave energy is in an early stage [6]. Commercial use is challenged by the high costs in design, installation, operation, and maintenance [7] and the difficulties in grid connection [8]. Integrating wave energy converters (WECs) [9]-[11] on a breakwater [12] to form a hybrid system has been proposed as a feasible way to help reduce the cost [13]. An exemplary commercial project is the Mutriku wave power plant [14] in the Bay of Biscay in Basque Country, Spain. 16 air chambers are set up in a

*Corresponding author
E-mail addresses: jinpeng@scut.edu.cn (P. Jin)

hollowed rubble mound breakwater functioned as oscillating water columns (OWCs) [15]-[17] and the plant is sufficient to power 250 households. Besides, in theoretical works such as Zheng *et al*. [18], Zheng *et al*. [19], Zhang *et al*. [20], Zhao *et al*. [21], Saeidtehrani *et al*. [22], and Cheng *et al*. [23], breakwater-WEC hybrid systems were evident to have better efficiency compared to the same WEC operating independently, making the use of wave power more cost-effective.

Among the various breakwater-WEC hybrid systems, one kind [24] consisting of point absorber wave energy converters (PAWECs) [25] deployed on the weather side of a floating pontoon breakwater has been reported to have several benefits. First, PAWECs have high energy conversion efficiency [26] and are easy to be arranged [27]. Second, compared with fixed breakwater, floating breakwater can be used in deep water regions, where wave energy density is much higher [28]. Third, PAWECs and floating breakwater have compatible functions and can benefit each other in a hybrid system. The presence of PAWECs blocks the direct wave impact on the floating breakwater and slightly reinforces its wave attenuation performance to offer a better shelter for the posterior infrastructures to be protected [20]. The presence of the floating breakwater influences the surrounding wave field to formulate a better energy harvesting environment for the PAWECs by focusing high waves [29][30]. Due to these advantages, such a hybrid system has recently become an active research area. Zhang *et al*. [20], Zhao *et al*. [31], Zhao and Ning [32], Reabroy *et al*. [33], Chen *et al*. [34], Zhang *et al*. [35], and Zhao *et al*. [36] studied hybrid systems containing a breakwater and a PAWEC, whereas Ning *et al*. [37], Zhao *et al*. [38], Tay [39], Zhang *et al*. [40] and Cheng *et al*. [41] studied hybrid systems containing a breakwater and an array of PAWECs. In most of these works, linear potential flow theory was applied to carry out a parametric study. The main concern was the influence of geometric factors such as the distance between the PAWECs and the breakwater on the hydrodynamic performance, power performance, and attenuation performance of the system.

In the above floating pontoon breakwater-PAWEC hybrid systems, the breakwater's functions are (1) keeping violent waves from relatively vulnerable infrastructures and (2) reflecting and focusing high waves for the PAWECs. In this sense, the breakwater is expected to have both good wave attenuation and focusing performance [29]. A lot of work has been done on the improvement of wave attenuation of a single floating pontoon. These methods could be roughly categorized into two groups. The first method is attaching auxiliaries such as trusses [42], porous plates [43], and nets [44] to the pontoons to dissipate incident wave energy by creating turbulence and vortices. The second method is to change the dimensions of a pontoon. The most effective way is enlarging the draft, which is particularly useful in dealing with relatively long waves [29]. Some works enlarge the draft of part of the pontoon instead of the entire. For instance, Zhang *et al*. [45] used a triangle-baffle-shaped bottom. Enlarging the width of a pontoon is another approach [29], although it is not as effective as enlarging the draft in most cases. Studies were working on changing the shape of the traditional rectangular pontoon as well, such as in refs. [29][46]-[48].

Due to the construction limits of a single large pontoon, a multi-pontoon design is

also applied. Dong *et al*. [49] compared a single-pontoon and a double-pontoon with the same width by experiment and showed that the double-pontoon was better in reducing wave height. Williams *et al*. [50] investigated a pair of long floating pontoon breakwaters of rectangular section, and found that "the wave reflection properties of the structures depend strongly on their width, draft and spacing, and the mooring line stiffnesses, while their excess buoyancy is of lesser importance." Similarly, Ning *et al*. [51] compared the performance of a single-pontoon breakwater and a dual-pontoon breakwater. They found that the width of the gap between the pontoons was crucial to the performance of the system. And the effective frequency range of the dual-pontoon breakwater wherein the transmission coefficient was smaller than 0.5 was wider than that of the single-pontoon breakwater. Ji *et al*. [52] proposed an innovative breakwater containing a pair of rectangular pontoons and meshes in between. It was compared with three other breakwaters and found to have the best wave attenuation performance. Configurations using more than two pontoons were also proposed. Guo *et al*. [53] found that in a triple-pontoon breakwater-WEC system, the width and draft of the front pontoon and the distance between the front pontoon and the middle pontoon had quite limited effect on the wave attenuation performance. Peng *et al*. [54] experimentally investigated the performance of a hybrid system consisting of a triple-pontoon breakwater-WEC and a fixed breakwater. Wave overtopping and breaking were observed on the top of the triple-pontoon and the hybrid system was proved effective in attenuating moderate and long waves. Zhao *et al*. [55] studied a multi-pontoon system with up to six pontoons and found that the wave attenuation performance in a multi-pontoon was superior compared with a single-pontoon. Zhang *et al*. [56] proposed a periodic array of caisson breakwater equipped with WECs and found that multiple-order propagating waves play an important role in both wave energy extraction and wave attenuation.

Compared to the rich work on the wave attenuation performance of a floating pontoon breakwater, its wave focusing performance is rarely mentioned. Zhang and Ning [57] proposed a design of several parabolic walls opening toward the weather side. Inspired by Zhang and Ning [30], Ren *et al*. [29] proposed a parabolic arc breakwater. Its superior wave attenuation and focusing performance were demonstrated and a critical frequency around which a much better attenuation could be achieved was observed. Mayon *et al*. [58] investigated the influence of a parabolic breakwater on a cylindrical OWC. Results show that both the efficiency and wave energy capture bandwidth are enhanced. Zhang *et al*. [40] used a large box-type pontoon to influence the wave field on the weather side of the breakwater and deployed WECs at several different locations to compare the power performance. The optimal deployment of the WEC array was also obtained based on the pattern of the focused wave field.

Although the wave attenuation performance of a multi-pontoon has been demonstrated, little is known about its wave focusing performance, particularly the influence of several key factors that are not available in a single-pontoon configuration. The novelties of this study are two folded. First, inspired by the work of Ren et al. [29], a parabolic pontoon twin-breakwater is proposed. Second, the wave attenuation and

focusing performance of the twin-breakwater is investigated, including the influences of the gap width and the connection method between the pontoons.

The rest of the paper is organized as follows. In Section 2, the mathematical model and a brief description of wave attenuation and focusing criteria are given. In Section 3, the influence of the gap width between the unconnected pontoons on its performance is studied. In Section 4, the influence of the gap width between the rigidly connected twin-breakwater on its performance is studied. In Section 5, a comparison between the connection methods is carried out. The conclusions are drawn in Section 6.

2. Methodology

2.1 Parallel twin-breakwater

As shown in Fig. 1, two parabolic pontoon breakwaters with the same dimensions are parallelly placed, denoted as BW#1 and BW#2. The pontoon geometry is defined by the chord length l, the uniform width w, the focal distance f, and the draft d. The distance between the two pontoons is denoted as the gap width w_{gap}. Moorings are not taken into account for the simplicity of the problem, as in ref. [20]. The water depth is denoted as h. Regular waves travel in the positive x-direction with a unit amplitude A and an angular frequency ω. In ref. [29], a parabolic pontoon with w=1 m, l=20 m, d=3 m, and f=10 m proved effective in both wave attenuation and focusing. Thereby in this study, the same layout is employed.

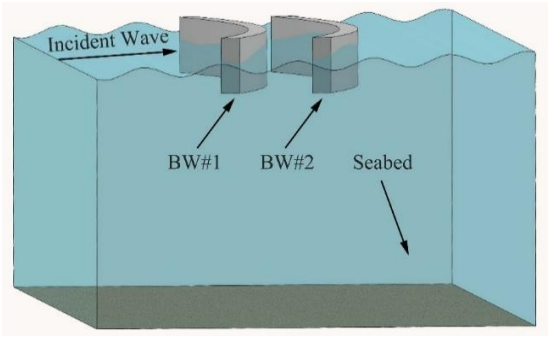

(a) 3D sketch

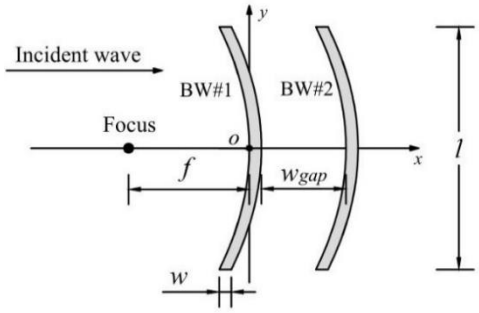

(b) top view

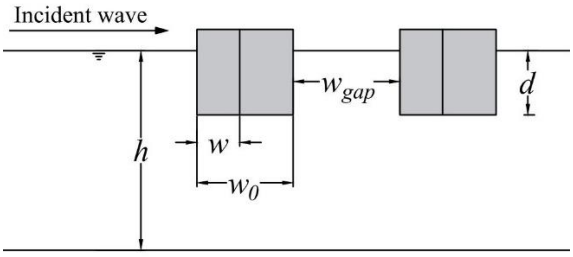

(c) side view

Fig. 1 Sketch of the parabolic twin-breakwater

2.2 Hydrodynamics

Interactions between waves and the twin-breakwater are simulated using the open-source code HAMS developed by Liu [59], incorporating an open-source package of free surface Green function [60]. The hydrodynamic fundamentals are similar to that in ref. [29]. This code is based on the linear wave theory. The fluid is assumed to be incompressible, inviscid, and the flow is irrotational, and the governing equation in the entire fluid domain is the Laplace equation:

$$\nabla^2\phi = 0 \tag{1}$$

The total velocity potential ϕ satisfies the following boundary conditions on the free surface S_f, the wet body surface S_b, and the seabed S_d (Fig. 1a):

$$\left.\begin{aligned} \frac{\partial\phi}{\partial z} &= \frac{\omega^2}{g}\phi \quad \text{on } S_f \\ \frac{\partial\phi}{\partial n} &= \mathbf{V}_n \quad \text{on } S_b \\ \frac{\partial\phi}{\partial z} &= 0 \quad \text{on } S_d \end{aligned}\right\} \tag{2}$$

where $\mathbf{V}_n$ is the normal component of the fluid velocity on the wet body surface S_b. The total velocity potential can be decomposed into three parts:

$$\phi = \phi_I + \phi_D + \phi_R \tag{3}$$

where ϕ_I is the incident velocity potential, ϕ_D is the diffraction velocity potential, and ϕ_R is the total radiation velocity potential. The problem can be solved in the frequency domain numerically by the Boundary Element Method using the open-source code HAMS. For a wave propagating in the positive x-direction, the incident potential is [29]

$$\phi_I = \frac{igA}{\omega}\frac{\cosh\left[k\left(z+h\right)\right]}{\cosh kh}e^{-ikx} \tag{4}$$

where $i^2=(-1)$. g is the acceleration of gravity. k is the wave number. ϕ_R can be written as follow:

$$\phi_R = -i\omega\sum_{j=1}^{6N}\xi_j\varphi_{Rj} \tag{5}$$

where ξ_j is the motion response and φ_{Rj} is the radiation potential in the jth motion mode of the twin-breakwater system oscillating with unit amplitude, respectively. N=1 while the two breakwaters are rigidly connected and N=2 while they are not connected.

The matrix form equation of motion can be written as:

$$\left[-\omega^2(\mathbf{M}+\mathbf{A})+i\omega\mathbf{B}+\mathbf{K}_s\right]\boldsymbol{\xi}=\mathbf{F}_e \tag{6}$$

where **M** is the mass matrices, **A** is the add mass matrices, **B** is the radiation damping matrices, and $\mathbf{K}_s$ is the hydrostatic stiffness matrices of the twin-breakwater system. $\mathbf{F}_e$ is the wave excitation force, and $\boldsymbol{\xi}$ is the motion response.

The complex surface elevation η can be obtained by:

$$\eta=\frac{\phi_I+\phi_D}{\mathrm{i}g/\omega}+\frac{\omega^2}{g}\sum_{j=1}^{6N}\xi_j\varphi_{Rj} \tag{7}$$

2.3 Performance criteria

For short incident waves, since the wave energy mainly concentrates on the water surface, it is easy for a floating breakwater to reflect the waves and protect the lee side. For incident waves with longer wavelengths, on the one hand, the waves would more easily pass through under a floating breakwater compared with the shorter waves. On the other hand, a floating breakwater will have a large motion response when it interacts with long waves, which may also induce a rise in wave height on the lee side. These are the main reasons why it is difficult for floating breakwaters to resist longer waves.

The wave attenuation and focusing performance criteria that have been established in ref [29] and are briefly introduced here for completeness. The deployment zone for the PAWECs and the protection zone for the protected infrastructures are shown in Fig. 2. 4141 (101 × 41) wave gauges are deployed in each zone. The discrete measurements by the gauges are fitted as a distribution of wave amplitude. In the deployment zone, the wave amplitude distribution illustrates the focal regions of high waves. An amplification factor a defined as the ratio of greatest amplitude to incident wave amplitude is also used to characterize the maximum wave focusing effect. In the protection zone, the average wave amplitude A_a is computed by taking the mean value of the wave amplitudes measured by the 4141 wave gauges. For the protection performance, the wave amplitude distribution and the average wave amplitude A_a are used to characterize both macroscopic and detailed features of the attenuation performance. More details about the performance criteria could be referred to ref [29].

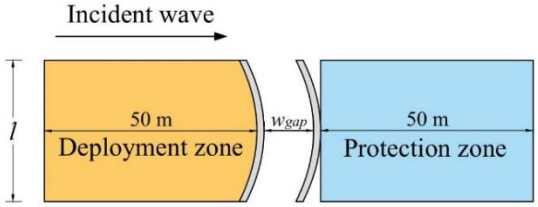

Fig. 2 Deployment zone and protection zone

3. Influence of gap width: unconnected pontoons

Here the two pontoons are unconnected and can oscillate in 6-DOF independently.

Five twin-breakwaters with w_{gap}=0, 2.0, 4.0, 6.0, 8.0 m are simulated. The water depth is h=15 m. The incident waves are from 0.1 rad/s to 3.5 rad/s with an increment of 0.01 rad/s. Fig. 3(a) shows that the incident waves from 0.1 rad/s to approximately 1.5 rad/s almost totally penetrate the twin-breakwaters, revealed by an average wave amplitude being around 1. For incident waves from approximately 2 rad/s to 3.5 rad/s, the attenuation performance of the twin-breakwaters becomes better as the incident frequency increases, and the average wave amplitude shows a general descending trend with fluctuations. On the one hand, as the fluctuations for different gap widths are different, they are likely caused by the complex diffraction induced by using two parallel breakwaters. On the other hand, one can find that the wave amplitude in the deployment zone is not uniformly distributed (Fig. 4). While some part in the deployment zone has large or small wave amplitudes, the calculated average wave amplitude is also influenced by the uneven distribution.

Similar to the findings in ref. [29], a particular frequency denoted as the critical frequency ω_c and the corresponding local minimum of wave amplitude denoted as the critical amplitude A_c could also be observed. The attenuation performance in the narrow band around the critical frequency is significantly improved. Such critical character is expected to be detected and applied. The critical frequencies ω_c for the unconnected twin-breakwaters with w_{gap}=0, 2, 4, 6, and 8 m are 1.68, 1.70, 1.70, 1.70, and 1.72 rad/s, respectively.

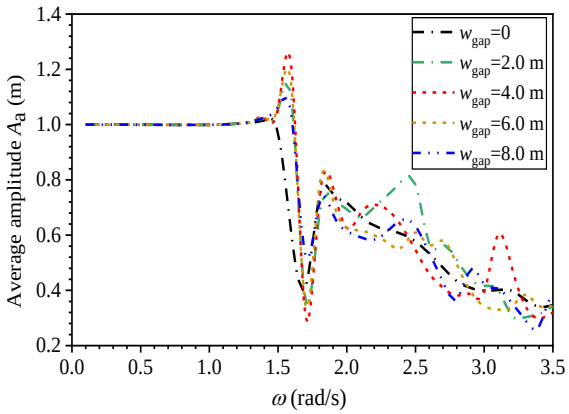

(a) average amplitude in waves

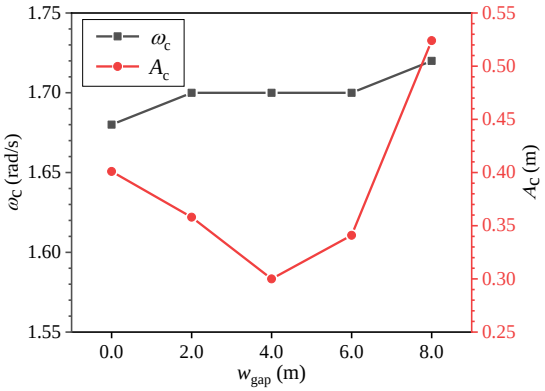

(b) critical frequency and critical amplitude of five unconnected twin-breakwaters

Fig. 3 Influence of gap width between the unconnected pontoons on wave attenuation and focusing performance

Results of the critical frequency and critical amplitude of the five unconnected twin-breakwaters are displayed in Fig. 3 (b). As the gap width increases from 0 to 8.0 m, the critical frequency slightly increases from 1.68 rad/s to 1.72 rad/s. On the one hand, this trend against the overall width is opposite to the findings in ref [29] that, for a single parabolic breakwater, an increase in width slightly decreases the critical frequency. The critical frequency is preferred lower for a potential dealing with longer waves. However, one cannot reduce the critical frequency of an unconnected twin-breakwater by increasing the gap width. On the other hand, the small change in the critical frequency despite a large difference in the gap width indicates that gap width has quite a limited effect on the critical frequency. Fig. 3 (b) also shows that as the gap width increases, the critical amplitude first decreases and then increases, and there is a minimum. Among the five cases, the minimum (0.301 m) occurs while w_{gap}=4 m, which is only 57.4% of that (0.524 m) while w_{gap}=8 m. Such a considerable reduction in the critical amplitude makes it worthwhile to search for the minimum by properly tuning the gap width. And the trifling variation of the critical frequency prevents an undesirable large increase.

The wave amplitude distributions in the protection zone at the critical frequency for each of the five unconnected twin-breakwaters are shown in Fig. 4. For a breakwater in 2D, a transmission coefficient of 0.5 is widely used as a criterion for effective attenuation. In this study of a breakwater in 3D, a modified version of the criteria is applied. The region where the amplitude is less than 0.5 m is regarded as an effective attenuation region [61], as shown by the contour lines in Fig. 4. Further, the region where the amplitude is less than 0.25 m is regarded as a prominent attenuation region and marked in Fig. 4 as well. The effective and prominent attenuation regions are preferred to be large with a regular shape for the convenience of placing infrastructures. From Fig. 3 (b) and Fig. 4, the area of effective attenuation region could be roughly reflected by the critical amplitude, i.e., smaller critical amplitude refers to a larger effective attenuation region. While w_{gap}=8.0 m, the effective attenuation region is the smallest, corresponding to the largest critical amplitude. The large effective attenuation regions for w_{gap}=2.0, 4.0, and 6.0 m are reflected by the corresponding small critical amplitude. The above findings indicate that the critical amplitude could be used for a primary estimation of attenuation performance. However, the shape of the effective attenuation region is not always reflected by the critical amplitude. As in the comparison between the w_{gap}=0 and w_{gap}=8.0 m cases, the effective attenuation region of the w_{gap}=8.0 m case is smaller but the shape is more regular. Thereby the shape of the effective attenuation region has to be examined case by case. The prominent attenuation region could also be roughly characterized by the critical amplitude. While w_{gap}=2.0, 4.0, 6.0 m, a large prominent attenuation region could be found around the x-axis. The w_{gap}=4.0 m case has the best attenuation performance among the five.

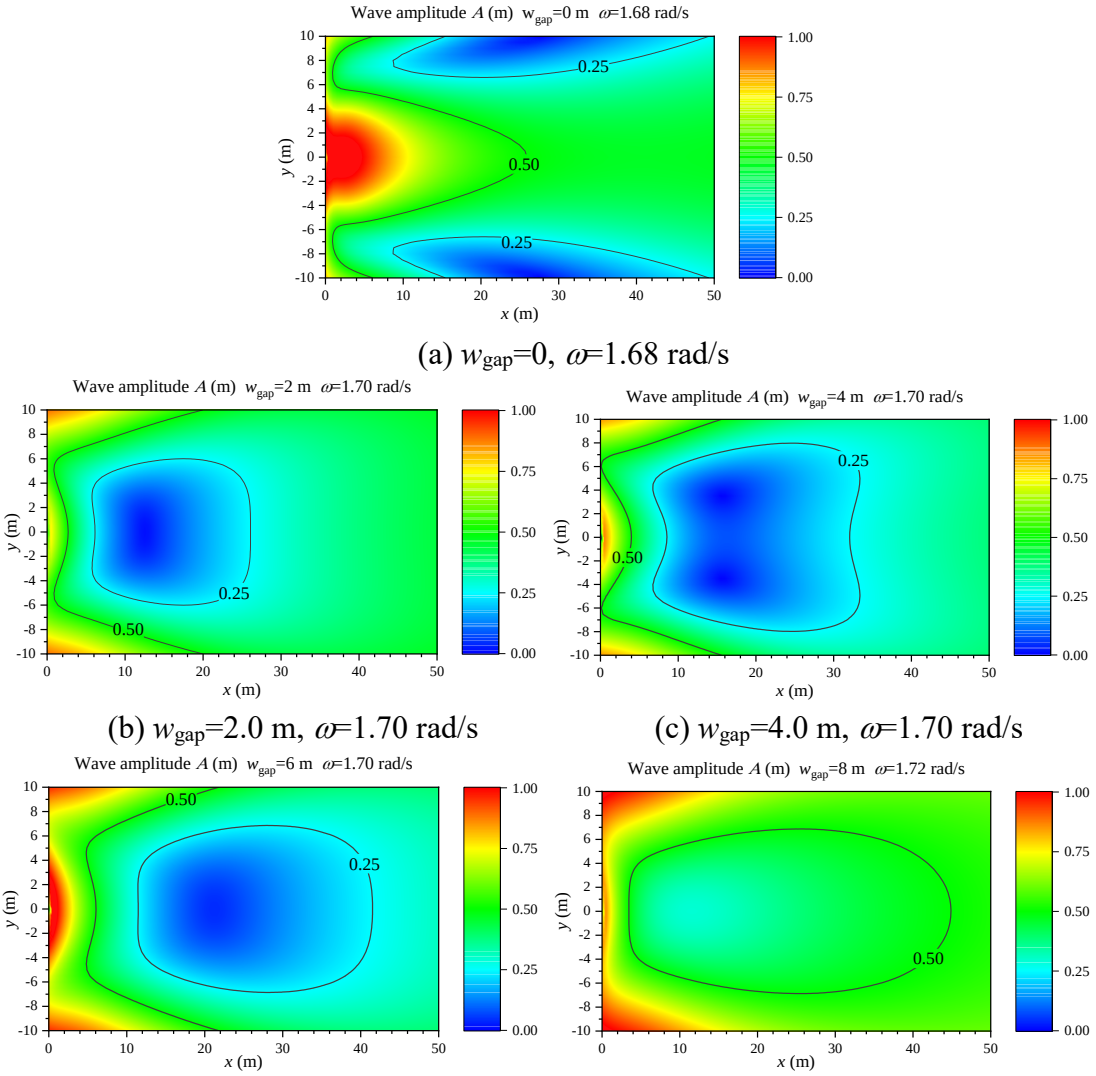

(a) w_{gap}=0, ω=1.68 rad/s

(b) w_{gap}=2.0 m, ω=1.70 rad/s

(c) w_{gap}=4.0 m, ω=1.70 rad/s

(d) w_{gap}=6.0 m, ω=1.70 rad/s

(e) w_{gap}=8.0 m, ω=1.72 rad/s

Fig. 4 Wave amplitude distribution in the protection zone of the unconnected twin-breakwaters under the critical frequency

The wave amplitude distributions in the development zone at the critical frequency for each of the five unconnected twin-breakwaters are shown in Fig. 5. The regions where the amplitude is greater than 2 m are circled and regarded as the high amplitude region as was done in ref [29]. The amplification factor a is also given. The reason for the amplification effect shown in Fig. 5 could be that a greater amount of wave energy is channeled by the parabolic wall to the centerline of the domain. A high amplitude region is preferred to be large with a regular shape to deploy larger or more PAWECs. Fig. 5 shows that gap width has a great influence on the wave focusing performance of an unconnected twin-breakwater. In general, the increase of gap width first improves and then worsens the wave focusing performance. An optimal wave focusing performance could be obtained for some gap width. While w_{gap}=0 and 8.0 m, there is no high amplitude region. While w_{gap}=2.0 m and w_{gap}=4.0 m, elliptical high amplitude regions appear, with an amplification factor up to 2.37. When w_{gap}=6.0 m, the high amplitude region shrinks to a small sectorial area. The high amplitude region could also be roughly reflected by the critical amplitude. Lower critical amplitude refers to a larger

high amplitude region and amplification factor. Note that the location of the high amplitude region is closer to the opening wall as the gap width increases, posing an advantage while using the breakwater as an installation foundation for the WECs.

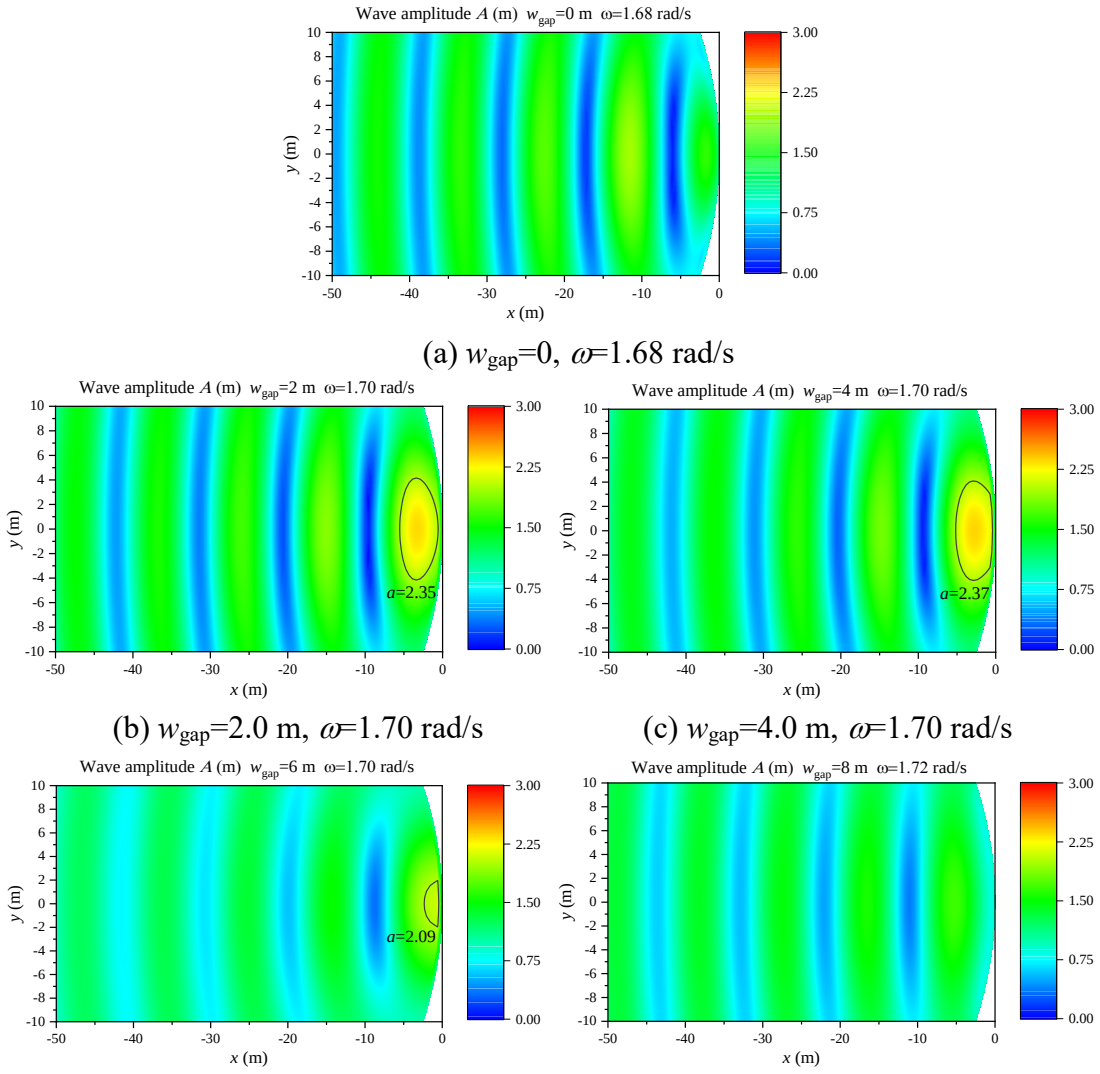

(a) w_{gap}=0, ω=1.68 rad/s

(b) w_{gap}=2.0 m, ω=1.70 rad/s

(c) w_{gap}=4.0 m, ω=1.70 rad/s

(d) w_{gap}=6.0 m, ω=1.70 rad/s

(e) w_{gap}=8.0 m, ω=1.72 rad/s

Fig. 5 Wave amplitude distribution in the deployment zone of the unconnected twin-breakwaters under the critical frequency

4. Influence of gap width: rigid connection between the pontoons

Here the two pontoons are rigidly connected. The other parameters are the same as those in Section 3. Fig. 6 shows that for a rigidly connected twin-breakwater, the critical nature also exists. Besides, while w_{gap}=4.0, 6.0, 8.0 m, a second dramatic drop of amplitude appears at an even lower frequency, denoted as the second critical frequency ω_{sc} and the second critical amplitude A_{sc}, respectively. In the following analysis, the features of the first and the second critical frequency are investigated.

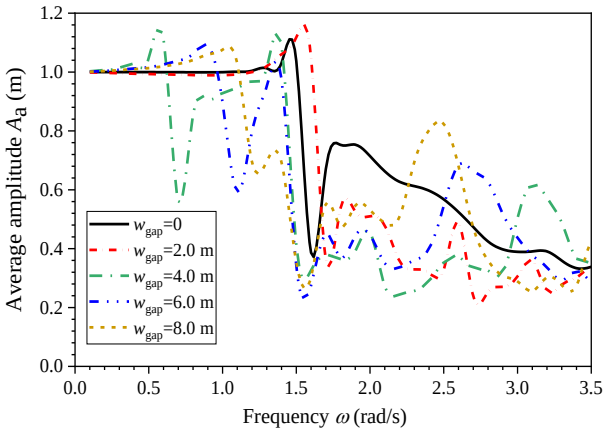

Fig. 6 Average amplitude in waves of five rigidly connected twin-breakwaters

4.1 First critical mode

Fig. 7(a) compares the first critical frequency and critical amplitude of the five rigidly connected twin-breakwaters. The critical frequency fluctuates between 1.58 rad/s and 1.70 rad/s as the gap width changes, showing no monotonic trend. This is mainly due to an extraordinary point that appears while w_{gap}=2.0 m. If it is not considered, the critical frequency first decreases and then increases, but the influence of gap width is quite small, similar to that in the unconnected twin-breakwaters. A minimum of the critical amplitude could be obtained while a proper gap width is chosen. In the present cases, the minimum (0.224 m) is obtained while w_{gap}=6.0 m, which is 41.51% lower than that (0.383 m) in the w_{gap}=0 case. Note that the minimum critical frequency and critical amplitude could be obtained for the same gap width, showing an advantage in the defense of long waves.

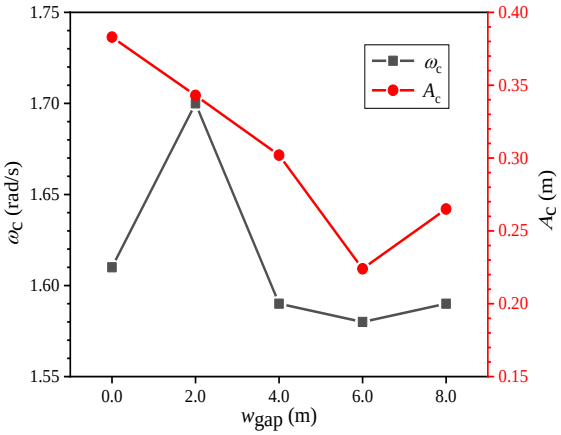

Fig. 7 Critical frequency and critical amplitude of five rigidly connected twin-breakwaters

The wave amplitude distributions in the protection zone at the first critical frequency for each of the five rigidly connected twin-breakwaters are shown in Fig. 8. Similar to that of the unconnected twin-breakwater, the areas of the effective attenuation region and the prominent attenuation region of a rigidly connected twin-breakwater can

be reflected by the critical amplitude, whereas their shapes still need further examination. Note that in the comparisons between the w_{gap}=4.0 m and w_{gap}=8.0 m cases, the critical amplitudes are approximately equal. The w_{gap}=8.0 m case has larger effective attenuation and prominent attenuation regions, but its prominent region is separated into two smaller ones, which may limit its use compared with the entire piece in the w_{gap}=4.0 m case. While w_{gap}=6.0 m, the protection zone is all an effective attenuation region and its prominent attenuation region is a large and entire piece, revealing the best attenuation performance in the five cases.

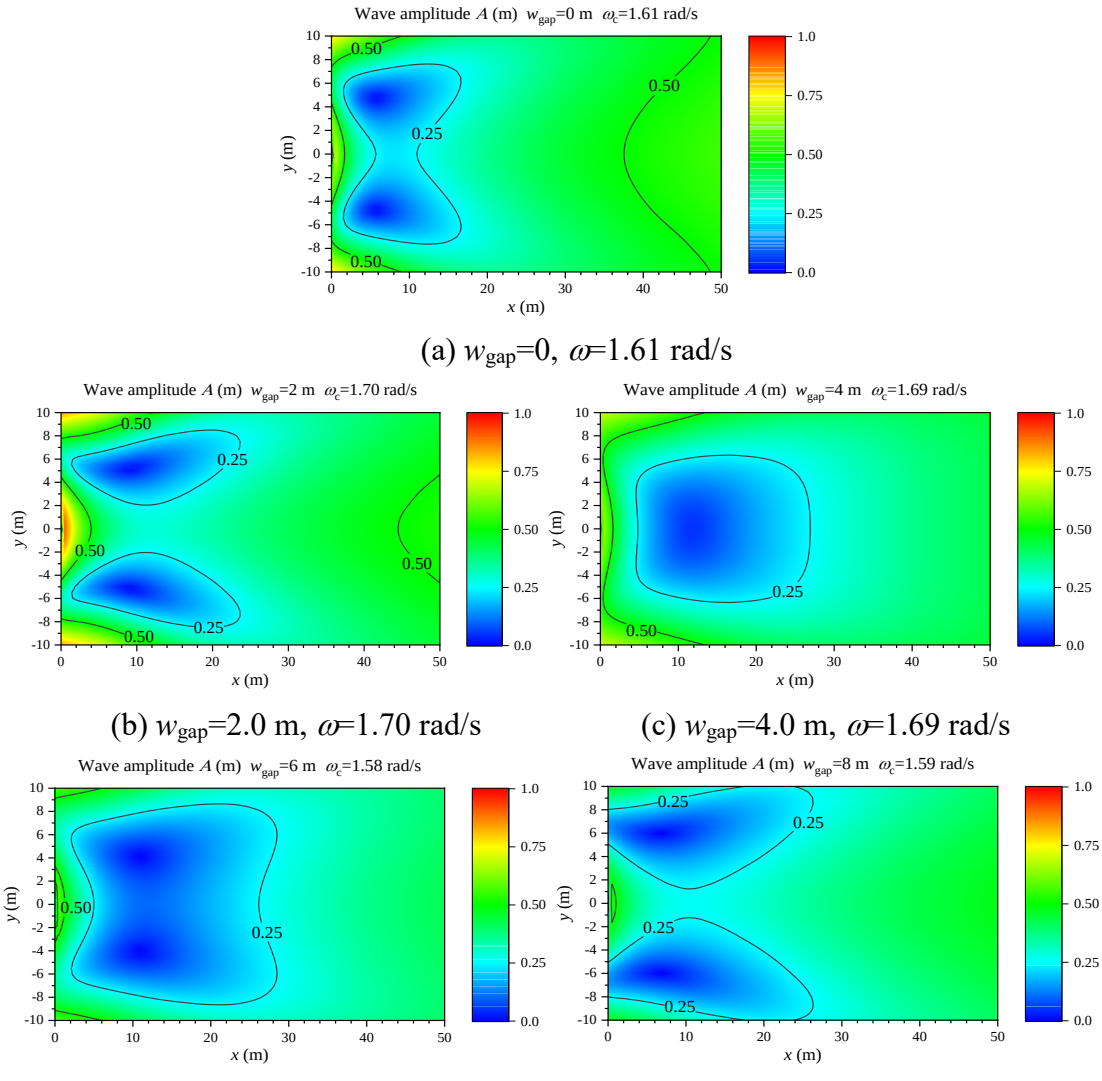

(a) w_{gap}=0, ω=1.61 rad/s

(b) w_{gap}=2.0 m, ω=1.70 rad/s

(c) w_{gap}=4.0 m, ω=1.69 rad/s

(d) w_{gap}=6.0 m, ω=1.58 rad/s

(e) w_{gap}=8.0 m, ω=1.59 rad/s

Fig. 8 Wave amplitude distribution in the protection zone of the rigidly connected twin-breakwaters under the critical frequency

The wave amplitude distributions in the development zone at the first critical frequency for each of the five rigidly connected twin-breakwaters are shown in Fig. 9. From Fig. 7 to Fig. 9, it is interesting that high wave focusing performance and high wave attenuation performance do not completely correspond to a rigidly connected twin-breakwater. For example, the w_{gap}=2.0 m case has the worst attenuation performance but the largest high amplitude region and amplification factor; the

w_{gap}=4.0 m and w_{gap}=8.0 m cases have nearly the same critical amplitude but different focusing performance; the w_{gap}=6.0 m case has the best attenuation performance but a mediocre focusing performance. Without considering the w_{gap}=2.0 m case, as the gap width increases, the area of the high amplitude region shrinks but the amplification factor increases. Similar to an unconnected twin-breakwater, a rigidly connected twin-breakwater with a positive gap width has its high amplitude region adjacent to the opening wall.

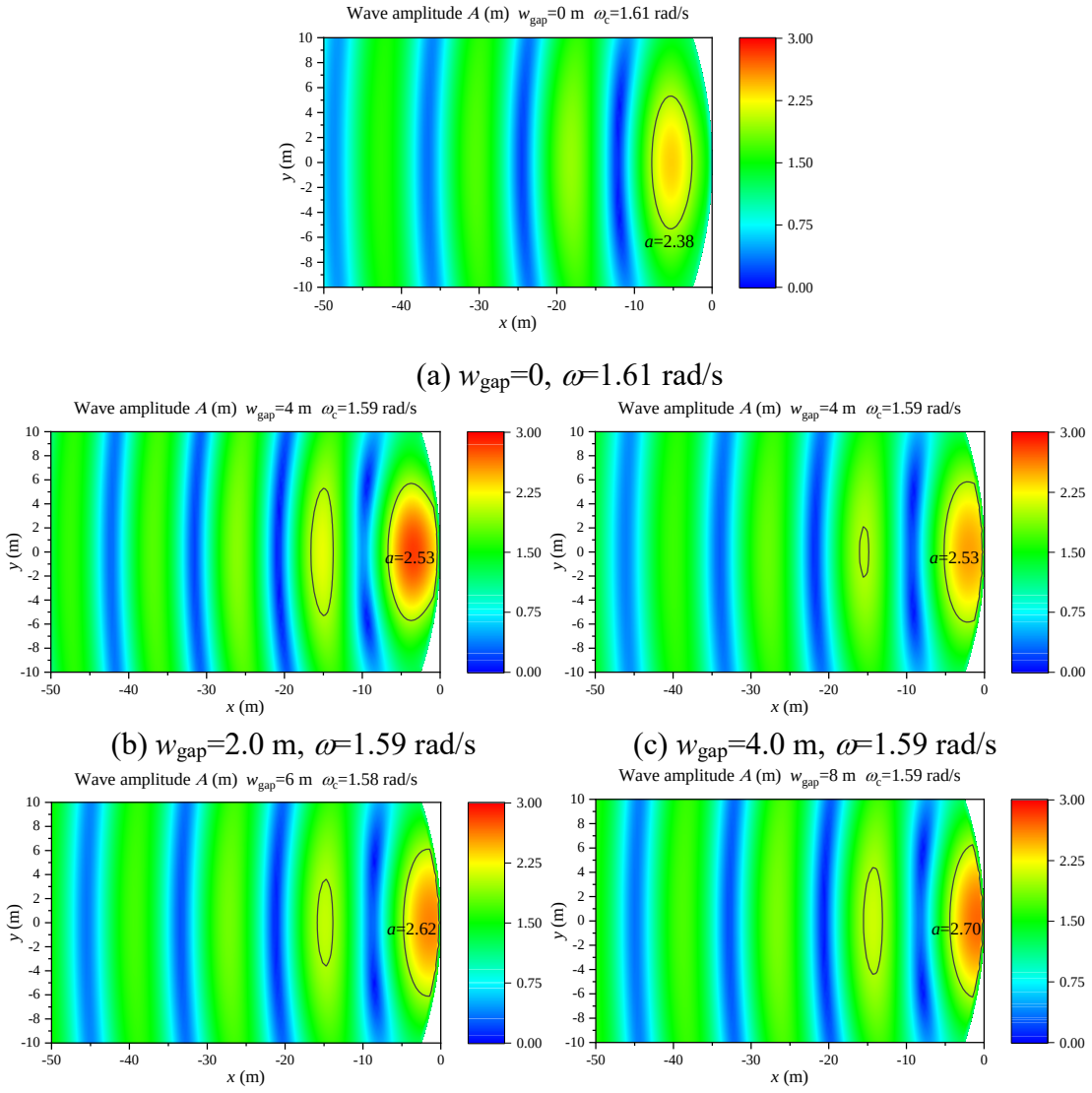

(a) w_{gap}=0, ω=1.61 rad/s

(b) w_{gap}=2.0 m, ω=1.59 rad/s

(c) w_{gap}=4.0 m, ω=1.59 rad/s

(d) w_{gap}=6.0 m, ω=1.58 rad/s

(e) w_{gap}=8.0 m, ω=1.59 rad/s

Fig. 9 Wave amplitude distribution in the deployment zone of the rigidly connected twin-breakwaters under the critical frequency

4.2 Second critical mode

The second critical frequency ω_{sc} and critical amplitude A_{sc} of the w_{gap}=4.0, 6.0, 8.0 m rigidly connected twin-breakwaters are shown in Fig. 10. They both increase as the gap width increases. Note that the second critical frequency of the w_{gap}=4.0 m case is 0.69 rad/s, indicating that the rigidly connected twin-breakwater has the potential to

defend long waves using the second critical mode.

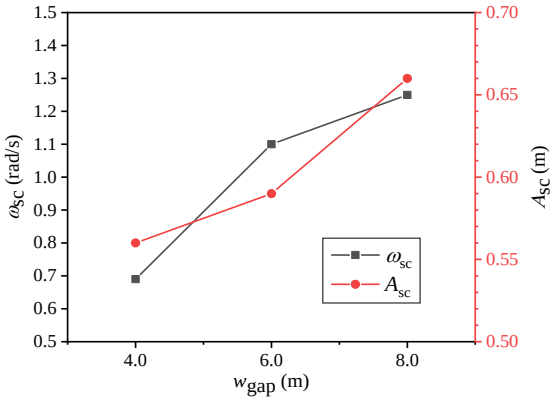

Fig. 10 Second critical frequency and critical amplitude of three rigidly connected twin-breakwaters

The wave amplitude distributions in the development zone and protection zone at the second critical frequency for the w_{gap}=4.0 m rigidly connected twin-breakwater are examined in Fig. 11. In the protection zone, an effective attenuation region could be found about 15 m behind the breakwater. This region is quite large and has a regular shape. In the deployment zone, no high amplitude region is found. Adjacent to the opening wall, a low amplitude region exists. These results show that while using the second critical mode for the defense of long waves, the attenuation performance could be satisfactory but the focusing performance might be sacrificed.

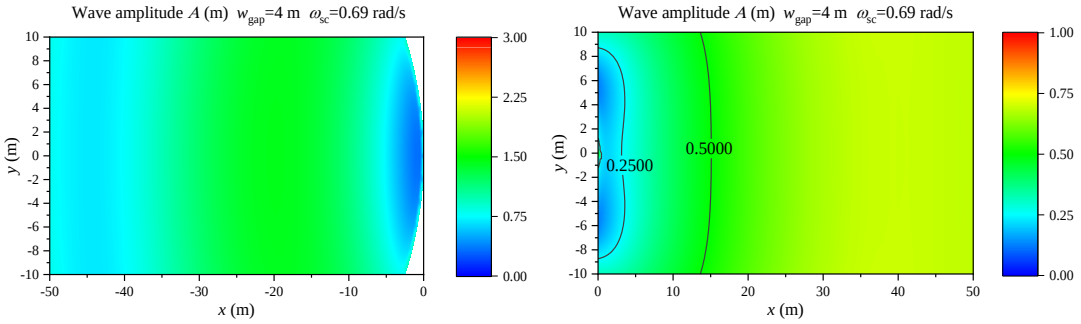

(a) in the deployment zone (b) in the protection zone

Fig. 11 Wave amplitude distribution in the deployment zone and protection zone of the w_{gap}=4 m rigidly connected twin-breakwater at the second critical frequency

5. Discussion on the connection method

In Section 3 and Section 4, the influence of gap width on the performance of unconnected and rigidly connected twin-breakwaters are respectively analyzed. In this section, a discussion on the connection method is addressed, with an emphasis on the performance difference it arouses. The comparative results of average wave amplitude for each pair of unconnected and rigidly connected twin-breakwaters with the same gap width are presented in Fig. 12. In most frequencies, the rigidly connected twin-breakwater is better in wave attenuation.

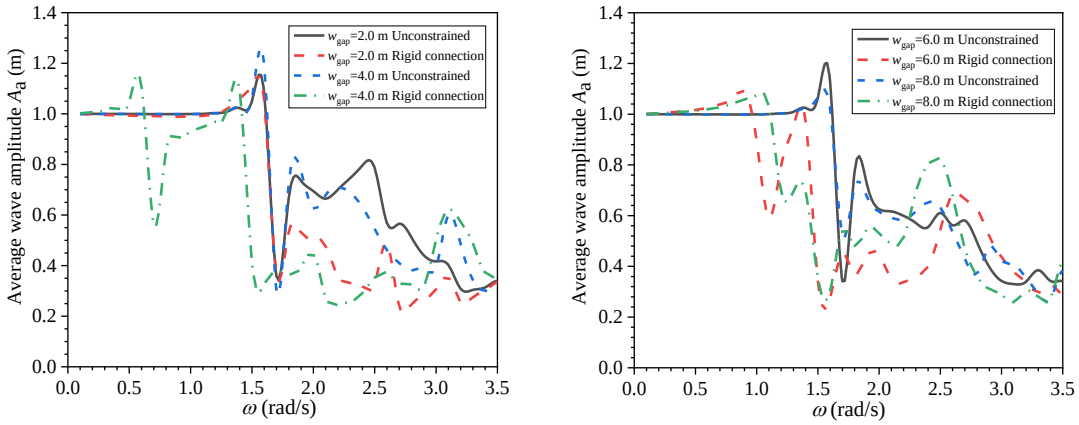

(a) w_{gap}=2.0 m and w_{gap}=4.0 m (b) w_{gap}=6.0 m and w_{gap}=8.0 m

Fig. 12 Average amplitude A_a in waves of each pair of unconnected and rigidly connected twin-breakwaters

From Fig. 3 (b) and Fig. 7, given a gap width, both the critical frequency and critical amplitude of the rigidly connected twin-breakwater are lower. In the unconnected twin-breakwaters, the trends of the critical frequency and critical amplitude against the gap width do not coordinate. The critical frequency slightly increases whereas the critical amplitude first decreases and then increases as the gap width increases. In contrast, these trends of the rigidly connected twin-breakwater coordinate well if the w_{gap}=2.0 m case is not considered. Such coordination creates an advantage that by fine-tuning, the minimum critical frequency and critical amplitude could be achieved simultaneously. Comparing Fig. 4 and Fig. 8, given a gap width, the areas of the effective and prominent attenuation regions of the rigidly connected twin-breakwater are both larger. Comparing Fig. 5 and Fig. 9, the area of the high amplitude region and the amplification factor of the rigidly connected twin-breakwater are also larger.

According to the above results, from the point of view of either wave attenuation or focusing, a rigid connection should be applied. One more thing that should be considered is that the wave attenuation and focusing performance of the rigidly connected twin-breakwater do not always coordinate, which does not happen to the unconnected twin-breakwater. The prominent attenuation region splits under some gap width. The high amplitude region gradually shrinks but the amplification factor increases as the gap width increases. Such incoordination may bring challenges while tuning the breakwater, which needs to be examined case by case. In the present configuration, the w_{gap}=6.0 m rigidly connected twin-breakwater has both optimal wave attenuation and focusing performance.

For both kinds of twin-breakwaters, the influence of gap width on the critical amplitude is much larger than on the critical frequency. One can focus on finding the minimum amplitude by changing the gap width without disturbing the corresponding critical frequency seriously.

6. Conclusion

A parabolic pontoon twin-breakwater is presented. The wave and breakwater interactions are modeled based on the potential linear theory in the frequency domain. The influences of the gap width and connection method between the two pontoons on the wave attenuation and focusing performance are investigated. The major conclusions are as follows.

(1) For an unconnected twin-breakwater, as the gap width increases, its critical frequency increases. A minimal critical amplitude could be obtained if a proper gap width is chosen. The wave focusing performance roughly coordinates with the wave attenuation performance, i.e., the best focusing and attenuation could be achieved simultaneously.

(2) For a rigidly connected twin-breakwater, as the gap width increases, if some particular value is not considered, both the critical frequency and critical amplitude first decrease and then increase. Their trends coordinate well. The minimal critical frequency and amplitude could be achieved simultaneously, posing an advantage in wave attenuation under proper tuning. The focusing performance does not coordinate well with the attenuation performance, but the deviation is not large.

(3) A second critical frequency occurs for some particular gap width of the rigidly connected twin-breakwater, showing potential in the defense of long waves.

(4) For both the unconnected and rigidly connected twin-breakwaters, the influence of gap width on the critical amplitude is much larger than on the critical frequency. One can focus on finding the minimum amplitude by changing the gap width without disturbing the corresponding critical frequency seriously. And the high amplitude region is closer to the opening for a larger gap width, posing an advantage in using the breakwater as an installation foundation.

(5) Under the same layout, a rigidly connected twin-breakwater is superior in both wave attenuation and focusing thereby being preferred.

Acknowledgment

This work is supported by the National Natural Science Foundation of China (52071096), National Natural Science Foundation of China National Outstanding Youth Science Fund Project (52222109), and Guangdong Basic and Applied Basic Research Foundation (2022B1515020036).

Reference

[1] Salter, S. H. (1974). Wave power. *Nature*, 249(5459), 720-724.

[2] Wang, S., Yuan, P., Li, D., & Jiao, Y. (2011). An overview of ocean renewable energy in China. *Renewable and Sustainable Energy Reviews*, 15(1), 91-111.

[3] Borthwick, A. G. (2016). Marine renewable energy seascape. *Engineering*, 2(1), 69-78.

[4] Mork, G., Barstow, S., Kabuth, A., & Pontes, M. T. (2010, January). Assessing the

global wave energy potential. In *International Conference on Offshore Mechanics and Arctic Engineering* (Vol. 49118, pp. 447-454).

[5] Gunn, K., & Stock-Williams, C. (2012). Quantifying the global wave power resource. *Renewable Energy*, 44, 296-304.

[6] Penalba, M., Giorgi, G., & Ringwood, J. V. (2017). Mathematical modelling of wave energy converters: A review of nonlinear approaches. *Renewable and Sustainable Energy Reviews*, 78, 1188-1207.

[7] Astariz, S., & Iglesias, G. (2015). The economics of wave energy: A review. *Renewable and Sustainable Energy Reviews*, 45, 397-408.

[8] O'Sullivan, D., & Dalton, G. (2009, September). Challenges in the grid connection of wave energy devices. In *8th European wave and tidal energy conference*. Uppsala, Sweden.

[9] Drew, B., Plummer, A. R., & Sahinkaya, M. N. (2009). A review of wave energy converter technology. *Proceedings of the Institution of Mechanical Engineers, Part A: Journal of Power and Energy*, 223(8), 887-902.

[10] Antonio, F. D. O. (2010). Wave energy utilization: A review of the technologies. *Renewable and Sustainable Energy Reviews*, 14(3), 899-918.

[11] Margheritini, L., Hansen, A. M., & Frigaard, P. (2012). A method for EIA scoping of wave energy converters—based on classification of the used technology. *Environmental Impact Assessment Review*, 32(1), 33-44.

[12] Dai, J., Wang, C. M., Utsunomiya, T., & Duan, W. (2018). Review of recent research and developments on floating breakwaters. *Ocean Engineering*, 158, 132-151.

[13] Mustapa, M. A., Yaakob, O. B., Ahmed, Y. M., Rheem, C. K., Koh, K. K., & Adnan, F. A. (2017). Wave energy device and breakwater integration: A review. *Renewable and Sustainable Energy Reviews*, 77, 43-58.

[14] Ibarra-Berastegi, G., Sáenz, J., Ulazia, A., Serras, P., Esnaola, G., & Garcia-Soto, C. (2018). Electricity production, capacity factor, and plant efficiency index at the Mutriku wave farm (2014–2016). *Ocean Engineering*, 147, 20-29.

[15] Falcão, A. F., & Henriques, J. C. (2016). Oscillating-water-column wave energy converters and air turbines: A review. *Renewable Energy*, 85, 1391-1424.

[16] Ning, D. Z., Zhou, Y., Mayon, R., & Johanning, L. (2020). Experimental investigation on the hydrodynamic performance of a cylindrical dual-chamber Oscillating Water Column device. *Applied Energy*, 260, 114252.

[17] Ning, D. Z., Shi, J., Zou, Q. P., & Teng, B. (2015). Investigation of hydrodynamic performance of an OWC (oscillating water column) wave energy device using a fully nonlinear HOBEM (higher-order boundary element method). *Energy*, 83, 177-188.

[18] Zheng, S., Zhang, Y., & Iglesias, G. (2019). Coast/breakwater-integrated OWC: A theoretical model. *Marine Structures*, 66, 121-135.

[19] Zheng, S., Antonini, A., Zhang, Y., Greaves, D., Miles, J., & Iglesias, G. (2019). Wave power extraction from multiple oscillating water columns along a straight coast. *Journal of Fluid Mechanics*, 878, 445-480.

[20] Zhang, H., Zhou, B., Vogel, C., Willden, R., Zang, J., & Geng, J. (2020).

Hydrodynamic performance of a dual-floater hybrid system combining a floating breakwater and an oscillating-buoy type wave energy converter. *Applied Energy*, 259, 114212.

[21] Zhao, X., & Ning, D. (2018). Experimental investigation of breakwater-type WEC composed of both stationary and floating pontoons. *Energy*, 155, 226-233.

[22] Saeidtehrani, S & Karimirad, M. (2021). Multipurpose breakwater: Hydrodynamic analysis of flap-type wave energy converter array integrated to a breakwater. *Ocean Engineering*, 235, 109426.

[23] Cheng, Y., Du, W., Dai S., Ji C., Collu, M., Cocard, M., Cui, L., Yuan, Z., Incecik, A. (2022). Hydrodynamic characteristics of a hybrid oscillating water column-oscillating buoy wave energy converter integrated into a π -type floating breakwater. *Renewable and Sustainable Energy Reviews*, 161, 112299.

[24] Zhao, X. L., Ning, D. Z., Zou, Q. P., Qiao, D. S., & Cai, S. Q. (2019). Hybrid floating breakwater-WEC system: A review. *Ocean Engineering*, 186, 106126.

[25] Jin, P., Zhou, B., Göteman, M., Chen, Z., & Zhang, L. (2019). Performance optimization of a coaxial-cylinder wave energy converter. *Energy*, 174, 450-459.

[26] Babarit, A. (2015). A database of capture width ratio of wave energy converters. *Renewable Energy*, 80, 610-628.

[27] Göteman, M. (2017). Wave energy parks with point-absorbers of different dimensions. *Journal of Fluids and Structures*, 74, 142-157.

[28] Hu, J., Zhou, B., Vogel, C., Liu, P., Willden, R., Sun, K., ... & Collu, M. (2020). Optimal design and performance analysis of a hybrid system combing a floating wind platform and wave energy converters. *Applied Energy*, 269, 114998.

[29] Ren, J., Jin, P., Liu, Y., & Zang, J. (2021). Wave attenuation and focusing by a parabolic arc pontoon breakwater. *Energy*, 217, 119405.

[30] Zhang, C., & Ning, D. (2019). Hydrodynamic study of a novel breakwater with parabolic openings for wave energy harvest. *Ocean Engineering*, 182, 540-551.

[31] Zhao, X., Ning, D., Zhang, C., Liu, Y., & Kang, H. (2017). Analytical study on an oscillating buoy wave energy converter integrated into a fixed box-type breakwater. *Mathematical Problems in Engineering*, 2017.

[32] Zhao, X., & Ning, D. (2018). Experimental investigation of breakwater-type WEC composed of both stationary and floating pontoons. *Energy*, 155, 226-233.

[33] Reabroy, R., Zheng, X., Zhang, L., Zang, J., Yuan, Z., Liu, M., ... & Tiaple, Y. (2019). Hydrodynamic response and power efficiency analysis of heaving wave energy converter integrated with breakwater. *Energy Conversion and Management*, 195, 1174-1186.

[34] Chen, Q., Zang, J., Birchall, J., Ning D., Zhao, X., Gao, J.(2020) On the hydrodynamic performance of a vertical pile-restrained WEC-type floating breakwater. *Renewable Energy*, 146, 414-425.

[35] Zhang, H., Zhou, B., Zang, J., Vogel, C., Fan, T., & Chen, C. (2021). Effects of narrow gap wave resonance on a dual-floater WEC-breakwater hybrid system. *Ocean Engineering*, 225, 108762.

[36] Zhao, X., Du, X., Li, M., & Göteman, M. (2021). Semi-analytical study on the hydrodynamic performance of an interconnected floating breakwater-WEC system

in presence of the seawall. *Applied Ocean Research*, 109, 102555.
[37] Ning, D. Z., Zhao, X. L., Chen, L. F., & Zhao, M. (2018). Hydrodynamic performance of an array of wave energy converters integrated with a pontoon-type breakwater. *Energies*, 11(3), 685.
[38] Zhao, X. L., Ning, D. Z., & Liang, D. F. (2019). Experimental investigation on hydrodynamic performance of a breakwater-integrated WEC system. *Ocean Engineering*, 171, 25-32.
[39] Tay, Z. Y. (2020). Performance and wave impact of an integrated multi-raft wave energy converter with floating breakwater for tropical climate. *Ocean Engineering*, 218, 108136.
[40] Zhang, H., Zhou, B., Zang, J., Vogel, C., Jin, P., & Ning, D. (2021). Optimization of a three-dimensional hybrid system combining a floating breakwater and a wave energy converter array. *Energy Conversion and Management*, 247, 114717.
[41] Cheng, Y., Xi, C., Dai, S., Ji, C., Collu M., Li, M., Yuan, Z., Incecik, A (2022). Wave energy extraction and hydroelastic response reduction of modular floating breakwaters as array wave energy converters integrated into a very large floating structure. *Applied Energy*, 306, 117953.
[42] Santo, H., Taylor, P. H., Day, A. H., Nixon, E., & Choo, Y. S. (2018). Current blockage and extreme forces on a jacket model in focused wave groups with current. *Journal of Fluids and Structures*, 78, 24-35.
[43] Koutandos, E. V., & Prinos, P. E. (2011). Hydrodynamic characteristics of semi-immersed breakwater with an attached porous plate. *Ocean Engineering*, 38(1), 34-48.
[44] Ji, C., Cheng, Y., Yang, K., & Oleg, G. (2017). Numerical and experimental investigation of hydrodynamic performance of a cylindrical dual pontoon-net floating breakwater. *Coastal Engineering*, 129, 1-16.
[45] Zhang, H., Zhou, B., Vogel, C., Willden, R., Zang, J., & Zhang, L. (2020). Hydrodynamic performance of a floating breakwater as an oscillating-buoy type wave energy converter. *Applied Energy*, 257, 113996.
[46] Duan, J. H., Cheng, J. S., Wang, J. P., & Wang, J. Q. (2012). Wave diffraction on arc-shaped floating perforated breakwaters. *China Ocean Engineering*, 26(2), 305-316.
[47] Chang, K. H., Tsaur, D. H., & Huang, L. H. (2012). Accurate solution to diffraction around a modified V-shaped breakwater. *Coastal Engineering*, 68, 56-66.
[48] Chu, Y. C., Cheng, J. S., Wang, J. Q., Li, Z. G., & Jiang, K. B. (2014). Hydrodynamic performance of the arc-shaped bottom-mounted breakwater. *China Ocean Engineering*, 28(6), 749-760.
[49] Dong, G. H., Zheng, Y. N., Li, Y. C., Teng, B., Guan, C. T., & Lin, D. F. (2008). Experiments on wave transmission coefficients of floating breakwaters. *Ocean Engineering*, 35(8-9), 931-938.
[50] Williams, A. N., Lee, H. S., & Huang, Z. (2000). Floating pontoon breakwaters. Ocean Engineering, 27(3), 221-240.
[51] Ning, D. Z., Zhao, X. L., Zhao, M., Hann, M., & Kang, H. G. (2017). Analytical investigation of hydrodynamic performance of a dual pontoon WEC-type

breakwater. *Applied Ocean Research*, 65, 102-111.

[52] Ji, C. Y., Chen, X., Cui, J., Gaidai, O., & Incecik, A. (2016). Experimental study on configuration optimization of floating breakwaters. *Ocean Engineering*, 117, 302-310.

[53] Guo, B., Wang, R., Ning, D., Chen, L., & Sulisz, W. (2020). Hydrodynamic performance of a novel WEC-breakwater integrated system consisting of triple dual-freedom pontoons. *Energy*, 209, 118463.

[54] Peng, W., Zhang, Y., Yang, X., Zhang, J., He, R., Liu, Y., & Chen, R. (2020). Hydrodynamic Performance of a Hybrid System Combining a Fixed Breakwater and a Wave Energy Converter: An Experimental Study. *Energies*, 13(21), 5740.

[55] Zhao, X., Xue, R., Geng, J., & Göteman, M. (2021). Analytical investigation on the hydrodynamic performance of a multi-pontoon breakwater-WEC system. *Ocean Engineering*, 220, 108394.

[56] Zhang, Y., Zhao, X., Geng, J., Göteman, M., Tao, L., (2022). Wave power extraction and coastal protection by a periodic array of oscillating buoys embedded in a breakwater. *Renewable Energy*, 190, 434-456.

[57] Zhang, C., & Ning, D. (2019). Hydrodynamic study of a novel breakwater with parabolic openings for wave energy harvest. *Ocean Engineering*, 182, 540-551.

[58] Mayon R., Ning D., Zhang C., Chen L., Wang R., (2021). Wave energy capture by an omnidirectional point sink oscillating water column system. *Applied Energy*, 304, 117795.

[59] Liu, Y. (2019). HAMS: A Frequency-Domain Preprocessor for Wave-Structure Interactions—Theory, Development, and Application. *Journal of Marine Science and Engineering*, 7(3), 81.

[60] Liu, Y., Yoshida, S., Hu, C., Sueyoshi, M., Sun, L., Gao, J., ... & He, G. (2018). A reliable open-source package for performance evaluation of floating renewable energy systems in coastal and offshore regions. *Energy Conversion and Management*, 174, 516-536.

[61] Ning, D. Z., Zhao, X. L., Zhao, M., Hann, M., & Kang, H. G. (2017). Analytical investigation of hydrodynamic performance of a dual pontoon WEC-type breakwater. *Applied Ocean Research*, 65, 102-111.